Permeation of macromolecules into the renal glomerular basement membrane and capture by the tubules

Marlon G. Lawrence[a,1], Michael K. Altenburg[a], Ryan Sanford[a], Julian D. Willett[a], Benjamin Bleasdale[a], Byron Ballou[b], Jennifer Wilder[a], Feng Li[a], Jeffrey H. Miner[c], Ulla B. Berg[d], and Oliver Smithies[a,2]

[a]Department of Pathology and Laboratory Medicine, The University of North Carolina at Chapel Hill, Chapel Hill, NC 27599-7525; [b]The Molecular Biosenser and Imaging Center, Carnegie Mellon University, Pittsburgh, PA 15213; [c]Division of Nephrology, Washington University School of Medicine, St. Louis, MO 63110-1093; and [d]Division of Pediatrics, Department of Clinical Science, Intervention and Technology, Karolinska Institutet, Karolinska University Hospital Huddinge, 14186 Stockholm, Sweden

Contributed by Oliver Smithies, December 9, 2016 (sent for review October 4, 2016; reviewed by Bruce A. Molitoris and Robert L. Reddick)

How the kidney prevents urinary excretion of plasma proteins continues to be debated. Here, using unfixed whole-mount mouse kidneys, we show that fluorescent-tagged proteins and neutral dextrans permeate into the glomerular basement membrane (GBM), in general agreement with Ogston's 1958 equation describing how permeation into gels is related to molecular size. Electron-microscopic analyses of kidneys fixed seconds to hours after injecting gold-tagged albumin, negatively charged gold nanoparticles, and stable oligoclusters of gold nanoparticles show that permeation into the lamina densa of the GBM is size-sensitive. Nanoparticles comparable in size with IgG dimers do not permeate into it. IgG monomer-sized particles permeate to some extent. Albumin-sized particles permeate extensively into the lamina densa. Particles traversing the lamina densa tend to accumulate upstream of the podocyte glycocalyx that spans the slit, but none are observed upstream of the slit diaphragm. At low concentrations, ovalbumin-sized nanoparticles reach the primary filtrate, are captured by proximal tubule cells, and are endocytosed. At higher concentrations, tubular capture is saturated, and they reach the urine. In mouse models of Pierson's or Alport's proteinuric syndromes resulting from defects in GBM structural proteins (laminin β2 or collagen α3 IV), the GBM is irregularly swollen, the lamina densa is absent, and permeation is increased. Our observations indicate that size-dependent permeation into the lamina densa of the GBM and the podocyte glycocalyx, together with saturable tubular capture, determines which macromolecules reach the urine without the need to invoke direct size selection by the slit diaphragm.

gel permeation | gold nanoparticles | slit diaphragm | Pierson's syndrome | Alport's syndrome

More than 50 y ago, Lathe and Ruthven described how the differential penetrance into swollen starch grains packed in a column could be used to separate substances in a size-dependent manner (1). Shortly thereafter, Ogston derived a simple equation relating the space available to molecules of differing sizes in a random network of fibers (2). More recently, Bosma and Wesselingh have rederived and extended Ogston's equation and have demonstrated its ability to describe the size-dependent permeation of a large range of macromolecules into a wide variety of gels (3). Subsequently, one of us hypothesized that excretion of proteins by the kidney is limited because macromolecules are excluded from the gel-like glomerular basement membrane (GBM) in proportion to their sizes and because most filtered macromolecules are removed by tubules unless capture is saturated (4).

Here, we tested this hypothesis by using confocal microscopy and transmission electron microscopy (TEM) to determine the permeation into the GBM and the subsequent fates of molecules of differing hydrodynamic radii. The confocal experiments showed that permeation into the GBM decreases as hydrodynamic size increases, in general agreement with Smithies/Ogston expectations. The TEM experiments, which enable quantification of the permeation into the different parts of the GBM, demonstrated the importance of the lamina densa and the podocyte glycocalyx in size selection and showed that small particles that can pass through the glomerulus are captured by proximal tubule cells and do not reach the urine unless this capture is saturated. Particles were observed at the luminal side of the podocyte glycocalyx, but none were seen adjacent to the slit diaphragm. In mouse models of Pierson's and Alport's syndromes, absence of either laminin β2 or collagen α3(IV) allowed the GBM to swell, precluded formation of a lamina densa, and increased permeation. We conclude that size-dependent permeation into the GBM and the podocyte glycocalyx, combined with saturable tubular capture of filtered macromolecules, determines whether macromolecules reach the urine. The slit diaphragm is essential for capillary structure but is probably not a direct determinant of glomerular size selectivity.

Results

Permeation into the GBM and Subsequent Fate of Fluorescent Macromolecules. Initial tests used confocal microscopy to determine the distribution in the kidney of fluorescent-tagged 12-kDa parvalbumin, 45-kDa ovalbumin, and 66-kDa BSA 2 min after their injection as a mixture into the tail veins of young adult male mice. The intensities of parvalbumin fluorescence in the GBM and in the

Significance

Human kidneys contain ~2 x 10^6 glomeruli that produce ~180 L per day of primary filtrate. Downstream tubules reabsorb most of the water, salt, and desirable low-molecular weight substances, leaving 1 to 2 L per day of urine containing undesirable waste products. Currently, most investigators think that the primary filtrate is low in protein because fluid exiting the glomerulus passes through slits spanned by a diaphragm that acts as a low-porosity molecular sieve. Our experiments challenge this view; they show that size-dependent permeation into the glomerular basement membrane and into a gel-like coat that covers the slits, together with saturable tubular reabsorption, determines which macromolecules reach the urine. The slit diaphragm is essential for capillary structure but may not directly determine glomerular size selectivity.

Author contributions: M.G.L., M.K.A., R.S., and O.S. designed research; M.G.L., M.K.A., R.S., J.D.W., B. Bleasdale, B. Ballou, J.W., F.L., J.H.M., U.B.B., and O.S. performed research; and M.G.L., M.K.A., and O.S. wrote the paper.

Reviewers: B.A.M., Indiana University School of Medicine; and R.L.R., University of Texas Health Science Center at San Antonio.

The authors declare no conflict of interest.

Freely available online through the PNAS open access option.

[1]To whom correspondence should be addressed. Email: lawrence_unc@outlook.com.

[2]Deceased January 10, 2017.

This article contains supporting information online at www.pnas.org/lookup/suppl/doi:10.1073/pnas.1616457114/-/DCSupplemental.

plasma were almost equal (Fig. 1*A*), indicating essentially unrestricted permeation into the GBM. The intensity of ovalbumin fluorescence in the GBM (Fig. 1*B*) was clearly less, and that of BSA was much less (Fig. 1*C*), demonstrating that permeation into the GBM is reduced as protein size increases. In Fig. 1*A*, parvalbumin fluorescence in the intracellular vesicles of the tall epithelial cells of a downstream proximal tubule (PT) is much brighter than in the GBM or the plasma, showing that substantial amounts of parvalbumin have passed through the glomerulus and have been captured by the tubules in the 2 min since the proteins were injected. In Fig. 1*B*, ovalbumin fluorescence in the GBM is less than that of parvalbumin although ovalbumin has still traversed the glomerulus and has been concentrated into intracellular vesicles within the proximal tubule cells. In Fig. 1*C*, no albumin fluorescence is visible in the tubules. Nevertheless, in other experiments, in which the kidneys were harvested from mice 15 min after injection, fluorescent-tagged BSA and IgG were detected in the intracellular vesicles of the proximal tubules, showing that glomerular filtration and tubular capture of these larger proteins occur, although detecting this capture requires a longer time of accumulation.

Both parvalbumin and ovalbumin were excreted in the urine (Fig. 1*D*), indicating that their capture by the proximal tubules was saturated. Interestingly, gel electrophoresis showed that the proteins in the urine at the early times were largely intact, but at the later times they were degraded. Far less fluorescent BSA was excreted, suggesting that tubular capture was adequate to capture the smaller amounts of this protein that had passed through the GBM.

The results of extensive measurements in unfixed whole-mount kidney preparations of the ratios of the intensities of fluorescence in the GBM and plasma (GBM/plasma intensities) of four fluorescent-tagged proteins and three fluorescent-tagged neutral dextrans are presented graphically in Fig. 1*E* (*SI Materials and Methods*, *Whole-Mount Fluorescence Measurements*). The panel is a plot of the natural logarithm of the experimentally determined ratios versus Ogston's variable $(R + r)^2$, where "R" is the hydrodynamic radius of the tested macromolecules and "r" is an assumed radius for the fibers comprising the gel (2, 4). The best fit line drawn through the experimental points accounts for 94% of the variance in the observed GBM/plasma ratios ($R^2 = 0.94$). We conclude that the concentrations in the GBM of the test molecules (including uncharged dextrans) are in general agreement with Ogston's permeation equation although the GBM/plasma ratios are large, ∼0.20 for albumin and ∼0.08 for 70-kDa dextran, because permeation into the lamina rara interna is only modestly restricted, as we show in *Size Discrimination by the GBM*, and because this region contributes most to the GBM fluorescence.

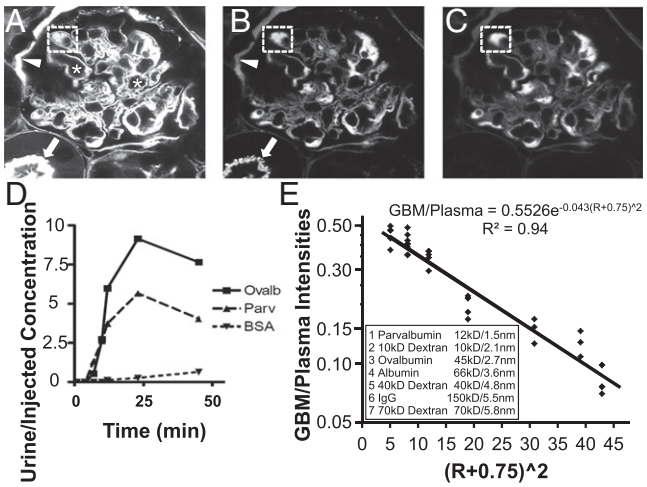

Fig. 1. The GBM/plasma ratio decreases as molecular size increases in general agreement with Ogston's equation; filtered proteins are captured by the proximal tubule, but some reach the urine. (*A*–*C*) Confocal images at appropriate wavelengths of a glomerulus in a paraformaldehyde-fixed kidney of a male mouse killed 2 min after tail-vein injection of parvalbumin (488 nm fluorophore), ovalbumin (555 nm), and BSA (647 nm). The overall brightness of the images has been adjusted so that the fluorescences for the three fluorophores are equal in a capillary that contains plasma (dotted square boxes). Many capillaries are devoid of plasma (asterisks) for reasons detailed in Fig. S2. The brush border of a proximal tubule is indicated with an arrow. The basement membrane of Bowman's capsule is indicated with an arrowhead. (*D*) Time course of the urinary concentration of the three proteins relative to their concentrations in the injected mixture. (*E*) Logarithmic plot of the GBM/plasma fluorescence intensities, measured in whole-mount unfixed kidneys, for four proteins and three dextrans versus the simple function, $(R + 0.75)^2$, of their hydrodynamic radii (R) expected from Ogston's equation (2, 4); molecular masses and Stokes/Einstein hydrodynamic radii are listed in the *Inset*.

Note that many of the glomerular capillaries in these images are devoid of plasma (Fig. 1*A*, asterisks). Instead, the capillary space is occupied by packed red cells or by the bodies of podocytes, endothelial cells, or mesangial cells (Figs. S1 and S2 and Table S1). Plasma retention was partially but never completely improved by injecting fixative under the kidney capsule before excision of the organ, as described by Farquhar et al., who had encountered the same problem (5).

Permeation of Gold-Tagged Albumin into the GBM. To better understand the events occurring in the GBM, we used transmission electron microscopy (TEM) to follow the fate of injected gold-tagged albumin and a variety of gold nanoparticles. This procedure required achieving a high concentration of particles in the glomerular capillaries, which we obtained by injecting them retrogradely via the superior mesenteric artery (*SI Materials and Methods*). Fig. 2*A* shows an Ag-enhanced TEM image obtained after arterial injection of mouse serum albumin tagged with 1.4-nm diameter gold nanoparticles (average ratio, one nanoparticle per albumin molecule). The gold-tagged mouse albumin is apparent in the plasma, but none is apparent in the GBM. Because the area of the GBM in the image is approximately one tenth the area of the plasma, this image shows that the GBM/plasma ratio for the tagged albumin was ≤0.1. To refine this estimate, we prepared two types of gold nanoparticles that are comparable with plasma proteins in hydrodynamic sizes and that do not agglutinate when administered at the high concentrations needed for counting macromolecules in regions within the GBM where permeation is low.

Sodium Borohydride Nanoparticles and Sodium Thiocyanate Oligoclusters. Sodium borohydride ($NaBH_4$) nanoparticles proved useful when made with hydrodynamic sizes up to that of ovalbumin (molecular mass 45 kDa); above that size, the preparations precipitated on storage. These near spherical nanoparticles were prepared (*SI Materials and Methods*) by a two-step alkaline reduction of 1 mM aqueous gold chloride—first with 3 mM or 5 mM DTT, then with 4 mM $NaBH_4$. They are stable in PBS made without calcium or magnesium but tend to irreversibly aggregate when at high concentrations in plasma or in PBS containing the divalent cations.

Sodium thiocyanate (NaSCN) oligoclusters proved useful when made in hydrodynamic sizes ranging from as small as albumin (molecular mass 66 kDa) to larger than IgG dimers (molecular mass 300 kDa). These oligoclusters were prepared by making 1 mM aqueous gold chloride alkaline, followed by adding the reductant, 10 mM NaSCN, after various delay times (6, 7). The oligoclusters, which are like bunches of grapes, comprise subunits ranging in number from 1 to over 50, the number being controlled by varying the delay time from less than a second to several hours. Once made, the oligoclusters are extremely stable. They have no tendency to aggregate even when at extremely high concentrations in plasma or PBS (6).

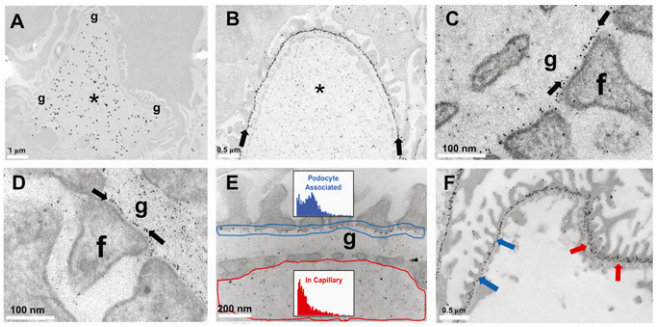

Fig. 2. Permeation of gold-tagged albumin and nanoparticles into the GBM and accumulation in a layer close to the bases of podocyte foot processes. (*A*) Enhanced TEM image of a glomerular capillary fixed immediately after retrogradely injecting gold-tagged mouse serum albumin into the superior mesenteric artery of a mouse under sublethal avertin anesthesia; the tagged albumin is plentiful in the plasma (asterisk); no albumin is observed in the GBM (g). (*B*) Enhanced image after injecting $NaBH_4$ gold nanoparticles comparable in size with ovalbumin; many particles (arrows) have accumulated within the GBM. (*C*) Higher magnification unenhanced image after injecting $NaBH_4$ nanoparticles; the particles within the GBM have actually accumulated close to the podocyte foot processes (f) though the podocyte associated particles (PAPs) are some distance from the podocyte plasma membrane. (*D*) Comparable magnification unenhanced image after injecting NaSCN oligoclusters; the oligoclusters also associate with the podocytes. (*E*, *Insets*) Histograms of sizes of particles in capillary plasma (outlined in red in the representative image behind the *Inset*) and of the particles associated with the podocytes (outlined in blue in the representative image); larger particles are overrepresented in the PAPs. (*F*) PAPs appear as a line (blue arrows) when viewed in cross-section although they appear as a layer when viewed in oblique sections (red arrows).

Both types of particles were coated with glutathione (GSH). The gold cores of the $NaBH_4$ particles have sharp outlines. The outlines of the NaSCN subunits are fuzzy, showing that they have a gold-containing fringe, which may account for their resistance to aggregation. When necessary for visualization in the TEM at lower magnifications, the gold cores of the $NaBH_4$ nanoparticles (but not the cores of the NaSCN oligoclusters) could be increased in size by enhancement with Ag before embedding, or, more conveniently, by Au enhancing ultrathin sections of London Resin (LR) white-embedded Karnovsky-fixed kidney samples on nickel grids.

The $NaBH_4$ Nanoparticles and NaSCN Oligoclusters Bind to a Component of the GBM Close to the Bases of the Podocyte Foot Processes. Fig. 2*B* shows an enhanced TEM image of a glomerular capillary after intraarterially injecting $NaBH_4$ nanoparticles comparable in size with ovalbumin, followed immediately by subcapsular injection of a fixative. As expected, these small nanoparticles permeated easily into the GBM. However, unexpectedly, many of them appeared at a high concentration close to the bases of the podocyte foot processes. Unenhanced images at a higher magnification show that these podocyte-associated particles (PAPs) are not directly adjacent to the plasma membrane of the podocytes (Fig. 2*C*); rather, they seem to be bound to a component of the GBM an appreciable distance upstream. NaSCN particles of a comparable size behave similarly (Fig. 2*D*). The size distribution of the PAPs differs from that of particles in the adjoining plasma (Fig. 2 *E* and *E*, *Inset*)—larger $NaBH_4$ particles are overrepresented even though we show in *Size Discrimination by the GBM* that permeation into the GBM favors smaller particles. The PAPs appear as a monomolecular line at the bases of the podocyte foot processes when viewed in cross-section (blue arrows in Fig. 2*F*), but oblique views show that they are actually a layer (red arrows in Fig. 2*F*).

Heparin Inhibits the Binding of the Particles to the GBM. Because both the $NaBH_4$ nanoparticles and the NaSCN oligoclusters have a high negative charge as a result of their GSH coats, we tested whether the binding might be blocked or reversed with heparin (which also has a high negative charge at physiological pHs), which proved to be the case. The usual binding (Fig. S3*A*) was completely blocked if 400 international units (I.U.) of heparin was injected via the tail vein before giving the particles (Fig. S3*B*). Likewise, heparin completely displaced the bound particles when given after the particles (Fig. S3*C*). The PAPs are so prevalent that further investigation is warranted to determine their relevance to normal glomerular function and their eventual fates.

Aggregates of $NaBH_4$ Nanoparticles Formed in Vivo. When small $NaBH_4$ nanoparticles were injected at high concentrations, the PAPs tended to form aggregates that were frequently observed at the entrance to the podocyte slits (Fig. 3*A*, black arrows), and less frequently at other sites along the bases of the podocyte foot processes (Fig. 3*A*, white arrow). (NaSCN oligoclusters did not form aggregates.) The number of particles in the aggregates varied from a few to more than 20. The aggregates were widely spaced along the slits (Fig. 3 *B* and *C*). The plane in which the aggregates located is highly informative. Thus, both the aggregates (Fig. 3*D*) and the individual particles (Fig. 3*E*) remaining in the glomerular capillaries an hour postinjection were in a plane that is clearly well upstream of the slit diaphragm, possibly at the luminal surface of the glycocalyx, which is present over the surfaces of the bases of the podocytes and covers the podocyte slits (8). Individual particles or aggregates of particles did not accumulate close to the slit diaphragm. The PAPs are persistent because they were still present in images obtained 2 and 4 h after the injection, at which times the plasma is virtually devoid of particles. No particles were seen within the podocytes at any time, indicating that they were not endocytosed by the podocytes. The PAPs did not dissociate easily because they were also present in kidneys that had been extensively perfused with room temperature PBS delivered from the heart, starting a few minutes after the injection.

Together, these results suggest that the aggregated PAPs cannot penetrate the glycocalyx of the podocytes but are swept to the podocyte slits by the tangential movement of fluid in the lamina rara externa, which is on its way to leaving the glomerulus via the slits. The PAPs are not endocytosed by the podocytes and remain for hours in a layer well upstream of the slit diaphragm.

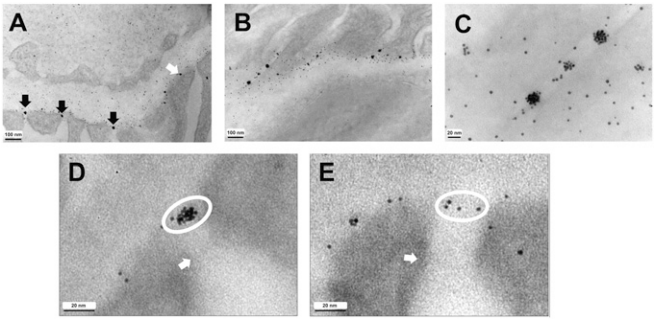

Fig. 3. When concentrated particles are injected, clusters of PAPs accumulate at the glomerular slits well upstream of the slit diaphragm, and the clusters can persist for minutes to hours. (*A*) Unenhanced cross-section of part of a glomerulus 5 min after arterially injecting concentrated small $NaBH_4$ nanoparticles. In vivo formed clusters of PAPs are seen at the podocyte slits (black arrows) and along the bases of the foot processes (white arrow). (*B*) En face view from the same kidney showing clusters along the slits. (*C*) Enlargement of *B* showing that the number of particles in the clusters is variable. (*D*) Cross-section 1 h after injecting small $NaBH_4$ nanoparticles. A large cluster of particles (white ellipse) is seen at this slit in a plane well upstream of the slit diaphragm (white arrow). (*E*) A neighboring slit in which a few individual particles appear in the same plane (white ellipse) well upstream of the slit diaphragm (white arrow). No particles are close to the slit diaphragm.

Size Discrimination by the GBM. Tests of the permeation properties of the GBM were made using NaSCN oligoclusters with narrow size distributions prepared by fractionating a pool of oligoclusters on a Superdex 200 column using PBS as the eluent buffer. On this column, fully-excluded Dextran 2000 eluted in fraction 20, and fully penetrant acetone eluted in fraction 49. The largest particles used in these GBM experiments eluted in fractions 22 to 24, approximately equivalent in hydrodynamic size to IgG dimers (molecular mass 300 kDa). The intermediate-sized particles eluted in fraction 28, approximately equivalent in size to IgG monomers (molecular mass 150 kDa). The smallest particles eluted in fractions 30 and 31, approximately equivalent in size to albumin (molecular mass 66 kDa).

TEM images were obtained of the GBM and adjoining plasma in the kidneys of mice injected intraarterially with the three sizes of particle, followed immediately by subcapsular injection of a fixative. The mice were pretreated with heparin to facilitate counting particles in the GBM uncluttered by the possible formation of PAPs. Note that, although the fixative is injected with minimal delay, fixation is slow compared with diffusion when submicron distances are involved, so that the images represent the state of the GBM at diffusion equilibrium. Fig. 4 *A*, *B*, and *C* shows representative images for the three sizes of particle. Fig. 4 *D*, *E*, and *F* shows the distributions of the particles across the GBM from the endothelium to the podocytes, obtained by counting particles in multiple images and assigning them to 17 bins. The large particles reached the lamina rara interna of the GBM, but none were observed in the lamina densa, and only 1 of 51 counted reached the lamina rara externa. The concentration of the large particles in the lamina rara interna was about one-third that in plasma ($4.6 \pm 0.4 \times 10^{-5}$ particles per unit area in lamina rara interna versus $14.7 \pm 2.5 \times 10^{-5}$ in upstream plasma, $P = 0.003$). Some of the intermediate-sized particles permeated into the lamina densa although only at about one-fifth their concentration in plasma ($6.1 \pm 2.1 \times 10^{-5}$ particles per unit area in the lamina densa versus $32.2 \pm 5.1 \times 10^{-5}$ in plasma, $P < 0.001$). The smallest-sized particles permeated into all parts of the GBM, with only a modest difference between the lamina rara interna and the lamina densa, which was no longer obvious; their concentrations in the lamina densa were about one-half that in plasma ($9.9 \pm 1.2 \times 10^{-4}$ per unit area in lamina densa versus $17.7 \pm 2.5 \times 10^{-4}$ in plasma, $P < 0.001$). Note the deficit of particles in the bin closest to the bases of the podocytes, supporting the postulate that permeation into the podocyte glycocalyx is restricted. No particles, large or small, were observed immediately upstream of the slit diaphragm.

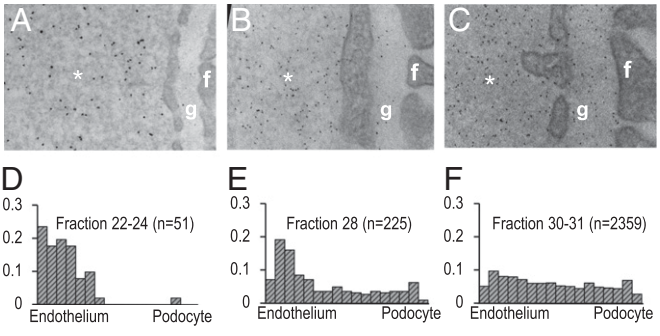

Fig. 4. Size discrimination by the GBM. (*A*) An unenhanced TEM image from a kidney fixed immediately after intraarterially injecting fraction 22 to 24 NaSCN oligoclusters into a heparinized mouse. The hydrodynamic size of these particles is comparable with that of IgG dimers. (*B*) GBM from a heparinized mouse that had received fraction 28 NaSCN oligoclusters approximately the size of IgG monomers. (*C*) GBM from a heparinized mouse that received fraction 30 and 31 NaSCN oligoclusters approximately the size of albumin. (*D–F*) Distributions of the three sizes of particle across the GBM from the endothelium to the bases of the podocytes; *n*, the number of particles of each size counted in the GBM. (*A–C*) Asterisks, plasma; f, podocyte foot process; g, GBM.

Genetically Determined Changes in GBM Permeation. Two human conditions in which albuminuria is caused by genetically determined changes in the major structural components of the GBM have been modeled in mice. One is Pierson's syndrome (9), a congenital nephrotic syndrome associated with ocular abnormalities; it is caused by mutations in *LAMB2*, the gene coding for the laminin β2 subunit. The other is Alport's syndrome (10), a progressive nephropathy characterized by hematuria, proteinuria, and GBM abnormalities; it is caused by mutations in the genes coding for the α3, α4, or α5 chains of type IV collagen. Mouse models of the two conditions have been made by disrupting the equivalent genes, *Lamb2* and *Col4a3* (11, 12). The Lamb2-null mice do not survive longer than a month, but their lifespan can be extended without losing the nephrotic syndrome if their podocytes express full-length rat laminin β2 cDNA with a mutation analogous to the pathogenic human LAMB2-R246Q mutation (B2LN-null) (13). Accordingly, we used these mice in our studies.

To test whether these mutations, which affect the structure of the GBM, alter its permeation, we used NaSCN oligoclusters prepared, as described (6, 7), with a delay time of 60 s. The resulting oligoclusters were monodisperse with a size approximating that of IgG monomers and a distribution sufficiently narrow for the oligoclusters to be used without fractionation.

Fig. 5 *A–C* presents typical TEM images of the GBMs from a WT mouse, the Pierson's model, and the Alport's model 2 min after tail-vein injection of the 60-s oligoclusters. In both models, we observed extensive disorganization and irregular increases in the thickness of the GBM, together with segmental podocyte foot process effacement. The distributions of the particles across the GBM in the three types of mouse are presented in Fig. 5 *D–F*. Permeation of the oligoclusters into the GBM is clearly altered in the mutants; there is no longer a region comparable with the lamina densa of WT mice that excludes the particles, indicating that the GBM in the mutant mice is less dense and less stratified than in the WT mouse. Fig. 5*G*, a plot of the GBM/plasma concentrations at 20 different locations along the glomerulus of a Pierson β2LN-null mouse, confirms this indication—permeation increases in direct proportion to the local thicknesses of the GBM ($R^2 = 0.53$). We conclude that absence of laminin β2, or of collagen α3(IV), major structural components of the GBM, precludes the formation of a lamina densa and allows the GBM to swell, which increases its permeability and therefore the transglomerular passage of macromolecules. This increased permeability and the accompanying podocyte foot process effacement probably both contribute to the proteinuria characteristic of the syndrome.

Saturable Capture of Filtered Particles by the Proximal Tubule. To explore further the factors that determine whether tubular capture of filtered nanoparticles is complete and the fate of any that are not captured, we injected a small readily filterable $NaBH_4$ nanoparticle at two doses, the lower dose being one-ninth of the higher. After 10 min, urines were collected and kidneys were imaged. Fig. 6 *A* and *B* shows that similar numbers of particles were captured and concentrated into intracellular vesicles by the proximal tubules of the lower and higher dose mice, despite the ninefold difference in the number of particles injected. In contrast, Fig. 6 *C* and *D* shows that the number of particles reaching the collecting ducts (and therefore the urine) was markedly dose-dependent. Thus, there were a large number of particles in collecting ducts from the higher dose mouse, but almost none in collecting ducts from the lower dose mouse. In agreement with this discordance, the urine of the higher dose mouse contained many particles whereas the urine of the low dose mouse had none. Together, these observations demonstrate the critical role of tubule reabsorption and its saturation in determining whether filtered macromolecules reach the urine.

Capture of Filtered Particles by Unusual Cells and by the Slit Diaphragm. In general, filtered particles are captured by the proximal tubules or are excreted in the urine when tubular capture is saturated.

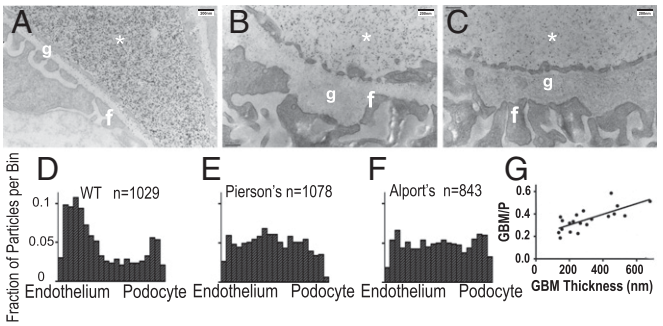

Fig. 5. The GBM is grossly and irregularly thickened but more permeable in mouse models of Pierson's and Alport's syndromes. (*A*) Unenhanced image of the GBM and adjoining plasma in the kidney of a heparinized WT mouse fixed 2 min after tail-vein injection of NaSCN oligoclusters comparable in size with IgG dimers. The GBM (g) is uniform in thickness. (*B*) Unenhanced image, at the same magnification as in *A*, of the GBM and adjoining plasma from a heparinized mouse model of Pierson's syndrome. The GBM is grossly and irregularly thickened up to three times that in WT. (*C*) An equivalent image from a heparinized mouse model of Alport's syndrome; the GBM shows the same gross and irregular thickening of the GBM as in the Pierson's model. (*D*) The distribution of particles across the GBM from the endothelium to the bases of the podocytes in the WT mouse. A region where the number of particles is at a minimum, the lamina densa, is clear. (*E*) The distribution in the Pierson's model; a region of low particle density is not present. (*F*) The distribution in the Alport's model. As in the Pierson's model, there is no region of low permeation. (*G*) A plot of the ratio of the number of particles per unit area in the GBM to the number of particles per unit area in the plasma (GMB/P) at 20 different locations along the GBM in a Pierson-model mouse; permeation increases in direct proportion to GBM thickness (R^2 = 0.53). (*A*–*C*) Asterisks, plasma; f, podocyte foot process; g, GBM; n, number of particles counted.

However, when the tubules are saturated, we have repeatedly observed intercalated cells in the collecting ducts that have captured large numbers of particles (Fig. S4*A*). We have also observed occasional proximal tubule cells with microvilli that bind unusually large numbers of particles (Fig. S4 *B* and *C*).

When the injected material contained very small GSH-coated particles that pass through the glomerulus and reach the primary filtrate, we routinely observed some particles apparently bound to the slit diaphragm. In cross-sectional views of glomerular capillaries, they appear as clusters at the level of the slit diaphragm (white ovals in Fig. S5*A*). Oblique views show that they are actually in monomolecular strings (white arrows in Fig. S5*B*). En face views show that the strings are located between the podocyte foot processes in a plane sufficiently distant from other structures and shallow enough to be imaged in a single section (Fig. S5*C*). The slit diaphragm apparently has a component that can bind very small gold nanoparticles.

Discussion

In the foregoing, we have described experiments aimed at testing whether differential permeation into the GBM and tubular reabsorption affect the kidney's ability to limit the urinary excretion of albumin and other macromolecules. We found the following. (*i*) Permeation into the GBM of fluorescent-tagged macromolecules was inversely related to their hydrodynamic size, in general agreement with Ogston's 1958 equation (2, 4) describing permeation into gels. (*ii*) Parvalbumin and ovalbumin passed through the glomerulus in amounts that saturated their capture by the tubules; uncaptured residues reached the urine; filtered albumin and IgG were fully captured and none reached the urine. (*iii*) Small negatively charged gold nanoparticles were observed bound to a component of the GBM close to the bases of the podocyte foot processes; heparin prevented and disrupted this binding. (*iv*) When high concentrations of the particles were injected, aggregates of a few to more than 20 particles were observed well upstream of the slit diaphragm; none were close to the slit diaphragm. (*v*) The aggregated podocyte-associated particles (PAPs) drifted to, but did not clog, the podocyte slits. (*vi*) The PAPs persisted for hours but were not endocytosed by the podocytes. (*vii*) Nanoparticles comparable in size with IgG dimers permeated into the lamina rara interna, but none were observed in the lamina densa. (*viii*) Nanoparticles comparable with IgG monomers permeated partially into the lamina densa, and some reached the lamina rara externa. (*ix*) Nanoparticles comparable with albumin permeated into all regions of the GBM, although at a lower concentration close to the bases of the podocytes. (*x*) Small nanoparticles injected at low concentration reached the primary filtrate but were almost completely captured by the proximal tubules; at higher concentrations, tubular capture was saturated and they reached the urine. (*xi*) Genetic absence of laminin β2LN or collagen α3 (IV) precluded the formation of a normal GBM with a lamina densa, thereby allowing the GBM to swell and increasing permeation in proportion to the swelling.

We conclude from these results that size-sensitive permeation into the lamina densa of the GBM and the podocyte glycocalyx, together with saturable capture by the proximal tubules, determines whether injected macromolecules reach the urine without the need to invoke size selection by the slit diaphragm. This conclusion agrees with that reached by Farquhar, Palade, and coworkers from their pioneering electron microscopic studies of the renal handling of ferritin and dextrans (5, 14), and with Comper's advocacy of the importance of proximal tubules in controlling albuminuria (15). It differs drastically from the currently widely accepted view, first advanced by Karnovsky and coworkers, that the slit diaphragm is the primary site of size discrimination because it has a zipper-like substructure with pores comparable in radius with that of albumin (16, 17).

Our findings that permeation into the lamina densa increases as hydrodynamic size decreases and that particles tend to be excluded from the podocyte glycocalyx are a strong argument for concluding that size selection occurs in the GBM. This conclusion does not dispute the great body of evidence demonstrating that nephrin is required for the formation of a slit diaphragm and normal glomerular function and that its absence in humans and in mice leads to nephrotic levels of proteinuria (18, 19). But it does

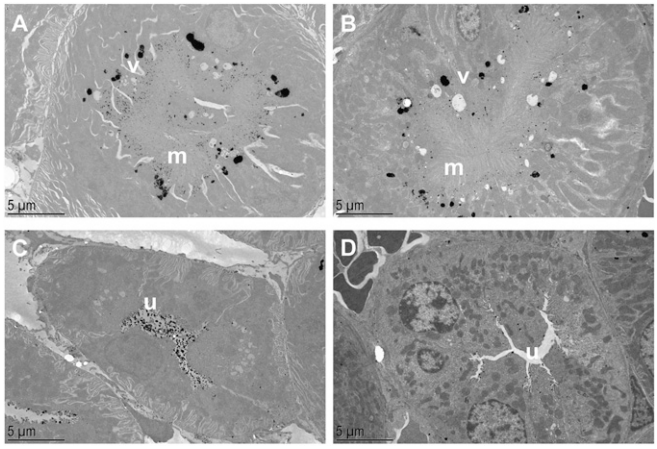

Fig. 6. Capture of filtered particles by the proximal tubule is saturable. (*A*) Enhanced image of a proximal tubule fixed 10 min after i.v. injection of $NaBH_4$ nanoparticles comparable in size with ovalbumin. Many filtered particles have been captured by the proximal tubule microvilli (m) and concentrated into intracellular vesicles (v). (*B*) A proximal tubule after injecting one-ninth the number of particles used for *A*. The number of captured particles and their location is similar to that in the higher dose mouse. (*C*) A collecting duct from a higher dose mouse. Many particles are in the urinary space (u), indicating that the capacity of the upstream proximal tubules to capture particles was saturated. (*D*) A collecting duct from the lower dose mouse. Almost no particles are in the collecting duct urinary space, indicating that the capacity of the upstream proximal tubules was not saturated.

dispute the conclusion that this evidence requires that the diaphragm is a size-sensitive filter, and we offer an alternative interpretation. Our interpretation is based on the premise that, regardless of its porosity, the slit diaphragm is necessary for glomerular capillary structure—it cross-links adjacent foot processes, fixes the width of the slits, and enables pulse pressure-sensitive compression of the GBM. When the diaphragm is absent, the podocyte foot processes are no longer properly conjoined, and glomerular filtration rate (GFR) is likely to be increased. Arguments have been presented elsewhere that substantially low GFRs can lead to proteinuria (4). In the reverse direction, Lazzara and Deen (20) have argued that substantially high GFRs can also lead to proteinuria because a high axial flow in the proximal tubules may leave insufficient residence time for all of the filtered protein to be captured before it is swept past the zone of capture. We suggest that a high GFR, rather than a failure of glomerular size selectivity, is the reason why mice and humans lacking a normal slit diaphragm are nephrotic. This interpretation is supported by measurements made on the renal status of four Finnish babies, lacking nephrin, while they were awaiting compatible kidney transplants. All had very high GFRs (determined as clearance of inulin) (21) as follows: girl 1 at 1 y of age had a GFR of 357 $mL{\cdot}min^{-1}{\cdot}1.73\ m^{-2}$; girl 2 at the age of 2.5 mo had a GFR of 223; girl 3 at 5 mo of age had a GFR of 95; girl 4 at 0.19, 0.64, 0.90, 1.09, and 1.66 y of age had GFRs of 137, 217, 198, 177, and 169. Normally, children will not reach a GFR of 100 until 1 y of age [Table S2, which also reports effective renal plasma flow (ERPF) measured as clearance of para-aminohippuric acid (PAH) (22) and serum creatinine levels (23)] (see also ref. 24). This interpretation of the data does not exclude the possibility that the slit-diaphragm acts as a molecular sieve, but it questions whether this action is required.

In summary, we have presented data showing the following: that a variety of proteins, dextrans, and gold nanoparticles permeate into the lamina densa in concentrations inversely related to their sizes, in general agreement with Ogston's well-tested gel-permeation equation; that tubular capture of filtered albumin and larger macromolecules normally prevents them from reaching the urine, but tubular capture is saturated when high doses of small proteins or small nanoparticles are injected; that permeation of gold nanoparticles into the lamina densa of the GBM and the podocyte glycocalyx is size-sensitive; that genetic absence of laminin β2 or collagen α3(IV), major structural proteins of the GBM, precludes formation of a lamina densa and allows gross and irregular swelling of the GBM, which increases permeation into the GBM in proportion to the swelling. We conclude that the lamina densa of the GBM and the podocyte glycocalyx together form the primary site of glomerular size discrimination, but that the saturable capture of filtered proteins and nanoparticles by the proximal tubule is critical in determining whether they reach the urine.

Materials and Methods

Male mice from a C57BL/6 genetic background were used in all studies. Injections were either via a tail vein in conscious mice or retrograde through the superior mesenteric artery of surgically prepared mice under general anesthesia. For general anesthesia, mice were given 0.3 to 0.5 mL of 2.5% (wt/vol) 2,2,2-tribromoethanol. The animals were handled under protocols approved by the Institutional Animal Care and Use Committees of the University of North Carolina at Chapel Hill. The patient studies were performed after informed consent by the parents, and the studies were approved by the Ethical Committee of Karolinska Institutet. Detailed protocols can be found in *SI Materials and Methods*.

Fluorescent-tagged proteins and dextrans used for i.v. injection were purchased from Invitrogen. They included the following: Alexafluor-488–labeled parvalbumin, Alexafluor-555–labeled ovalbumin, Alexafluor-647–labeled BSA, tetramethylrhodamine (TMR)-labeled 10-kDa, 40-kDa, and 70-kDa dextrans. Protocols for synthesis of $NaBH_4$ and NaSCN gold nanoparticles can be found in *SI Materials and Methods* and refs. 6 and 7, respectively.

After injection with fluorescent-tagged proteins or dextrans, various sized gold nanoparticles, or gold-tagged mouse serum albumin (Nanoprobes), the left kidney was harvested and prepared for either confocal microscopy or TEM as described in *SI Materials and Methods*.

ACKNOWLEDGMENTS. We thank C. Robert Bagnell and Vicky J Madden for help and guidance in electron microcopy; and Thomas M. Coffman, J. Charles Jennette, and Nobuyo Maeda for encouragement, help, and advice. This work was supported by NIH Grants HL 49277, DK078314, and DK100593.

1. Lathe GH, Ruthven CR (1955) The separation of substances on the basis of their molecular weights, using columns of starch and water. *Biochem J* 60(4):xxxiv.
2. Ogston AG (1958) The spaces in a uniform random suspension of fibers. *Trans Faraday Soc* 54:1754–1757.
3. Bosma JC, Wesselingh JA (2000) Partitioning and diffusion of large molecules in fibrous structures. *J Chromatogr B Biomed Sci Appl* 743(1-2):169–180.
4. Smithies O (2003) Why the kidney glomerulus does not clog: A gel permeation/diffusion hypothesis of renal function. *Proc Natl Acad Sci USA* 100(7):4108–4113.
5. Farquhar MG, Wissig SL, Palade GE (1961) Glomerular permeability. I. Ferritin transfer across the normal glomerular capillary wall. *J Exp Med* 113:47–66.
6. Smithies O, et al. (2014) Stable oligomeric clusters of gold nanoparticles: preparation, size distribution, derivatization, and physical and biological properties. *Langmuir* 30(44):13394–13404.
7. Lawrence M, Testen A, Koklic T, Smithies O (2016) A simple method for the size controlled synthesis of stable oligomeric clusters of gold nanoparticles under ambient conditions. *J Vis Exp* 2016(108):e53388.
8. Roth J, Brown D, Orci L (1983) Regional distribution of N-acetyl-D-galactosamine residues in the glycocalyx of glomerular podocytes. *J Cell Biol* 96(5):1189–1196.
9. Zenker M, et al. (2004) Congenital nephrosis, mesangial sclerosis, and distinct eye abnormalities with microcoria: An autosomal recessive syndrome. *Am J Med Genet A* 130A(2):138–145.
10. Alport AC (1927) Hereditary familial congenital haemorrhagic nephritis. *BMJ* 1(3454): 504–506.
11. Noakes PG, et al. (1995) The renal glomerulus of mice lacking s-laminin/laminin beta 2: nephrosis despite molecular compensation by laminin beta 1. *Nat Genet* 10(4): 400–406.
12. Miner JH, Sanes JR (1996) Molecular and functional defects in kidneys of mice lacking collagen alpha 3(IV): Implications for Alport syndrome. *J Cell Biol* 135(5):1403–1413.
13. Chen YM, Kikkawa Y, Miner JH (2011) A missense LAMB2 mutation causes congenital nephrotic syndrome by impairing laminin secretion. *J Am Soc Nephrol* 22(5):849–858.
14. Farquhar MG (1975) Editorial: The primary glomerular filtration barrier–basement membrane or epithelial slits? *Kidney Int* 8(4):197–211.
15. Comper WD (2014) Albuminuria is controlled primarily by proximal tubules. *Nat Rev Nephrol* 10(3):180.
16. Karnovsky MJ, Ainsworth SK (1972) The structural basis of glomerular filtration. *Adv Nephrol Necker Hosp* 2:35–60.
17. Rodewald R, Karnovsky MJ (1974) Porous substructure of the glomerular slit diaphragm in the rat and mouse. *J Cell Biol* 60(2):423–433.
18. Kestilä M, et al. (1998) Positionally cloned gene for a novel glomerular protein–nephrin–is mutated in congenital nephrotic syndrome. *Mol Cell* 1(4):575–582.
19. Putaala H, Soininen R, Kilpeläinen P, Wartiovaara J, Tryggvason K (2001) The murine nephrin gene is specifically expressed in kidney, brain and pancreas: Inactivation of the gene leads to massive proteinuria and neonatal death. *Hum Mol Genet* 10(1):1–8.
20. Lazzara MJ, Deen WM (2007) Model of albumin reabsorption in the proximal tubule. *Am J Physiol Renal Physiol* 292(1):F430–F439.
21. Hilger HH, Klümper JD, Ullrich KJ (1958) Wasserrückresorption und Ionentransport durch die Sammelrohrzellen der Säugetierniere. *Pflugers Arch* 267(3):218–237.
22. Smith HW, Finkelstein N, Aliminosa L, Crawford B, Graber M (1945) The renal clearances of substituted hippuric acid derivatives and other aromatic acids in dog and man. *J Clin Invest* 24(3):388–404.
23. Masson P, Ohlsson P, Björkhem I (1981) Combined enzymic-Jaffé method for determination of creatinine in serum. *Clin Chem* 27(1):18–21.
24. Heilbron DC, Holliday MA, al-Dahwi A, Kogan BA (1991) Expressing glomerular filtration rate in children. *Pediatr Nephrol* 5(1):5–11.